

Applying Chebyshev-Tau spectral method to solve the parabolic equation model of wide-angle rational approximation in ocean acoustics

Houwang Tu, Yongxian Wang, Xian Ma and Xunjiang Zhu

*College of Meteorology and Oceanography, National University of Defense Technology,
Changsha, 410073, China
tuhouwang96@163.com
yxwang@nudt.edu.cn*

Received (3 Dec 2020)

Revised (Day Month Year)

Solving an acoustic wave equation using a parabolic approximation is a popular approach for many available ocean acoustic models. Commonly used parabolic equation (PE) model programs, such as the range-dependent acoustic model (RAM), are discretized by the finite difference method (FDM). Considering the idea and theory of the “split-step” parabolic approximation, a discrete PE model using the Chebyshev spectral method (CSM) is derived, and the code is developed. We use the problems of two ideal fluid waveguides as examples, i.e., one with a constant sound speed in shallow water and one with a Munk sound speed profile in the deep ocean. The correctness of the discrete PE model using the CSM to solve a simple underwater acoustic propagation problem is verified. The test results show that compared with the finite difference discrete PE model, the proposed method in this paper has a higher accuracy in the calculation of underwater acoustic propagation in a simple marine environment and requires fewer discrete grid points. However, the proposed method has a longer running time than the finite difference discrete PE program. Thus, it is suitable to provide high-precision reference standards for the benchmark examples of the PE model.

Keywords: Chebyshev-Tau; spectral method; parabolic approximation, ocean acoustics.

1. Introduction

The ocean is rich in energy, minerals and biological resources. The urgent requirements of marine research and development have posed new challenges in the detection, identification, positioning and communication of underwater targets. Sound waves are currently the main means of remotely transmitting information underwater; therefore, it is of great practical significance to thoroughly study and understand the laws of underwater acoustic propagation. As a mathematical expression of acoustic physical properties, computational acoustic fields can describe the physical laws of ocean sound propagation with simple and clear numerical solutions. Extensively used ocean acoustic field calculation theories include the parabolic equation (PE) model, normal modes, the wavenumber integration method and ray.¹ The PE model has the advantage of being fast and flexible when solving range-dependent sound propagation issues. In the 1970s, Hardin and Tappert^{2,3} introduced the PE method to underwater acoustics for the first time, and they approximated the Helmholtz equation into a two-dimensional equation that was related to only the range and depth

and irrelevant to the azimuth. In the 1980s, Davis et al derived a generalized PE model using the method of the operator.⁴ The derivation based on a series expansion of square-root operator Q opens the path to formulate better PE approximations with a wide-angle capability. Greene⁵ and Clearbout⁶ selected different coefficients and derived their respective large-angle PE models. The interest in PE techniques has steadily grown within the ocean acoustic modeling community. Based on the idea of parabolic approximation, many parabolic model schemes have been proposed,^{7–10} and more types of PE models may be found in references.^{11–13} Bamberger et al presented a generalized very-wide-angle PE based on a Padé series expansion.¹⁴ Collins first implemented the wide-angle PE numerical solution based on the high-order Padé approximation^{15,16} and expanded the propagation angle to nearly 90°. This process solved many practical problems such as the self-starter to obtain an initial condition,¹⁷ “split-step” high-order Padé series approximation,¹⁸ energy loss problem caused by step approximation^{19–21} and treatment of the inclined seafloor boundary. Then, the classic underwater acoustic propagation calculation program RAM is developed. The depth operator is discretized using the finite difference method (FDM). This approach to replace the depth operator with a tridiagonal matrix handles piecewise continuous depth variations in the acoustic parameters.²² After discretizing in-depth, the numerical solution involves repeatedly solving tridiagonal systems of equations. Although the FDM is the main method for numerical simulations in underwater acoustic field (RAM, FOR3D, FFP, KRAKEN, Bellhop), it still has many shortcomings and deficiencies. For example, the FDM is difficult to construct high-precision difference schemes, and the convergence and stability of complex numerical schemes are difficult to mathematically verify. The equidistant grid used by FDM can cause smaller information than the grid size to be ignored. To satisfy the rapidly growing requirements of various underwater acoustic applications, the development of new discrete methods with high accuracy and rapid calculations has important scientific and application value. In scientific computing and engineering numerical simulation, the spectral method (SM) is one of three major numerical discrete methods juxtaposed with the FDM and finite element method.^{23,24} The SM is frequently used in various mathematical and physical problems such as computational fluid dynamics problems, chemical measurements, and electricity because of its high accuracy.^{22,25,26} The SM originates from the method of weighted residuals. It uses orthogonal polynomials (triangular polynomials, Chebyshev polynomials, Legendre polynomials, etc.) as the basis functions, series expansion to approximate the variables to be solved, and finite-order truncation. The greatest advantage of the SM is that it has “infinity convergence”, i.e., when the solution of the original equation is sufficiently smooth, the approximate solution obtained by the SM will quickly converge to the exact solution. In recent decades, the SM has been vigorously developed and is an important tool for solving differential equations.²⁷ Some researchers have begun to apply the SM to solving acoustic problems. Colbrook²⁸ presented a new approach to solve acoustic scattering problems. Wise²⁹ represented an arbitrary acoustic source and sensor distributions in Fourier collocation methods. Wang et al³⁰ presented an improved expansion scheme for the acoustical wave propagator. Evans³¹ proposed a Legendre-Galerkin technique for differential eigenvalue problems with complex and discontinuous coefficients in under-

water acoustics. Subsequently, Evans³² studied the Legendre-Galerkin spectral method to construct atmospheric acoustic normal modes. Tu et al³³ implemented a Chebyshev-Tau spectral method to solve acoustic normal modes with a stratified ocean. In applying the spectral method to solve the parabolic equation model, Tu et al³⁴ presented the standard PE model using the Chebyshev spectral method (CSM) to process a single layer of a body of water with constant density and no attenuation. At present, there is no research to introduce the SM to solve the PE model of wide-angle rational approximation. This study attempts to introduce the CSM into the solution of the PE model in underwater acoustics, designs two examples, and analyzes and compares the advantages and shortcomings of the proposed CSM-based PE model in terms of calculation accuracy and running time.

2. Derivation of the PE model

Consider a cylindrical coordinate system where the sound source is a simple harmonic point source and the marine environment is a cylindrically symmetric two-dimensional sound propagation case, Helmholtz equation can be written as:

$$\left[\frac{\partial^2}{\partial r^2} + \frac{1}{r} \frac{\partial}{\partial r} + \rho \frac{\partial}{\partial z} \left(\frac{1}{\rho} \frac{\partial}{\partial z} \right) + k_0^2 n^2 \right] \tilde{P} = 0, \quad (1)$$

where ρ is the density, c_0 is the reference sound speed, f is the frequency of the sound source, $k_0 = 2\pi f/c_0$ is the reference wavenumber, $n = c_0/c$ is the refractive index, and \tilde{P} is the acoustic pressure in the frequency domain. For long-distance sound propagation, sound waves are generally approximated as cylindrical waves. According to the attenuation law of cylindrical waves, the energy amplitude of the sound wave is proportional to \sqrt{r} . To eliminate the extension term, the following coordinate transformation is introduced for the acoustic pressure in Eq. (1):

$$p = \sqrt{r} \tilde{P}. \quad (2)$$

Substituting Eq. (2) into Eq. (1), we obtain:

$$\frac{\partial^2 p}{\partial r^2} + \rho \frac{\partial}{\partial z} \left(\frac{1}{\rho} \frac{\partial p}{\partial z} \right) + k_0^2 n^2 p + \frac{p}{4r^2} = 0. \quad (3)$$

By applying far-field approximation $k_0 r \gg 1$ to Eq. (3), we know:

$$k_0^2 n^2 p \gg \frac{p}{4r^2}. \quad (4)$$

After discarding the small item $\frac{p}{4r^2}$, we can rewrite Eq. (4) as follows:

$$\frac{\partial^2 p}{\partial r^2} + \rho \frac{\partial}{\partial z} \left(\frac{1}{\rho} \frac{\partial p}{\partial z} \right) + k_0^2 n^2 p = 0. \quad (5)$$

When considering attenuation, let wavenumber $k = (1 + i\eta\beta)\omega/c(z)$, where $c(z)$ is the speed of sound, $\omega = 2\pi f$ is the circular frequency, β is the attenuation in dB/wavelength, i is the imaginary unit, and $\eta = (40\pi \log_{10} e)^{-1}$. We introduce the operator decomposition

4 *H. Tu et al.*

method proposed by Lee et al⁷ to factorize Eq. (5) and rewrite it in the form of outwardly propagating waves and inwardly propagating waves:

$$\left(\frac{\partial}{\partial r} - ik_0\sqrt{1+X}\right)\left(\frac{\partial}{\partial r} + ik_0\sqrt{1+X}\right)p + \left[\frac{\partial}{\partial r}, ik_0\sqrt{1+X}\right] = 0, \quad (6)$$

where depth operator X is:

$$X = k_0^{-2} \left[\rho(z) \frac{\partial}{\partial z} \left(\frac{1}{\rho} \frac{\partial}{\partial z} \right) + k^2 - k_0^2 \right]. \quad (7)$$

When we ignore the horizontal change of the medium parameter, the derivative terms of $\left[\frac{\partial}{\partial r}, ik_0\sqrt{1+X}\right]$ in the above formula can be exchanged, so the simplified form of Eq. (6) is as follows:

$$\left(\frac{\partial}{\partial r} - ik_0\sqrt{1+X}\right)\left(\frac{\partial}{\partial r} + ik_0\sqrt{1+X}\right)p = 0. \quad (8)$$

Among the two terms of Eq. (8), the former part represents waves propagating outwards, the latter part represents waves propagating inwards, and the inward propagation is negligible. Then, we obtain the parabolic equation of the following form:

$$\frac{\partial p}{\partial r} = ik_0\sqrt{1+X}p. \quad (9)$$

According to the solving method of ordinary differential equations, the step solution of the equation can be obtained as:

$$p(r + \Delta r, z) = \exp\left(ik_0\Delta r\sqrt{1+X}\right)p(r, z), \quad (10)$$

where Δr is the step size in the horizontal direction. Collins used the Padé series expansion method,¹² where an n -term rational function is used to approximate the exponential function in Eq. (10):

$$p(r + \Delta r, z) = \exp(ik_0\Delta r) \prod_{j=1}^n \frac{1 + \alpha_{j,n}X}{1 + \beta_{j,n}X} p(r, z), \quad (11)$$

n is the number of items used for the rational approximation; the choice will also affect the accuracy of the approximation. More precisely, it is determined by the user according to the complexity of the research environment and characteristics of the sound source. The calculation of complex coefficients $\alpha_{j,n}$ and $\beta_{j,n}$ must satisfy the requirements of stability, convergence and accuracy.

To numerically solve Eq. (11), depth operator X must be discretized. Traditionally, FDM is usually used to discretize and form a set of tridiagonal matrix algebraic equations. This article intends to use the CSM to solve the PE model.

3. CSM for the PE model

3.1. Chebyshev spectral method

The SM is a kind of the weighted residual method, it is based on finite-order expansion and summation to approximate the unknown function to be sought. Any sufficiently continuous and smooth unknown function $u(x)$ is expanded by a set of smooth basis and weighted sum. Essentially, this set of basis forms a function space, and the so-called expansion can also be understood as a projection. The SM using Chebyshev orthogonal polynomials as the basis functions is the CSM, in which the basis functions $T_k(x)$ are:

$$\begin{aligned} T_0(x) &= 1; & T_1(x) &= x; & T_2(x) &= 2x^2 - 1 \\ T_{k+1}(x) &= 2xT_k(x) - T_{k-1}(x) & k &= 2, 3, 4, \dots \end{aligned} \quad (12)$$

Any smooth and differentiable unknown function $u(x), x \in [-1, 1]$ can be expanded by those infinite basis functions and approximated by the finite sum of the first $N + 1$ terms:

$$u(x) = \sum_{k=0}^{\infty} \hat{u}_k T_k(x) \approx \sum_{k=0}^N \hat{u}_k T_k(x). \quad (13)$$

The expansion coefficient can be obtained by the following formula:

$$\hat{u}_k = \frac{2}{\pi c_k} \int_{-1}^1 \frac{u(x) T_k(x)}{\sqrt{1-x^2}} dx, \quad c_k = \begin{cases} 2, & k = 0 \\ 1, & k > 0 \end{cases}. \quad (14)$$

Eqs. (14) and (13) are the so-called forward Chebyshev transform and backward Chebyshev transform, respectively.

The integral in Eq. (14) is usually calculated numerically. The method of Gaussian quadrature is generally considered to have high accuracy. Considering the accuracy of the numerical quadrature and the convenience of processing boundary conditions, the Chebyshev-Gauss-Lobatto points are often used:

$$x_j = \cos\left(\frac{j\pi}{N}\right), \quad j = 0, 1, 2, \dots, N, \quad (15)$$

where $N + 1$ is the number of discrete points, which is equal to the truncated order in CSM. When the $N + 1$ Chebyshev-Gauss-Lobatto points are used, the expansion coefficient \hat{u}_k in Eq. (15) can be approximately obtained as:

$$\begin{aligned} \hat{u}_k &\approx \frac{1}{d_k} \sum_{j=0}^N u(x_j) T_k(x_j) \omega_j, \quad k = 0, 1, 2, \dots, N \\ \omega_j &= \begin{cases} \frac{\pi}{2N}, & j = 0, N \\ \frac{\pi}{N}, & \text{otherwise} \end{cases}, \quad d_k = \begin{cases} \pi, & k = 0, N \\ \frac{\pi}{2}, & \text{otherwise} \end{cases}. \end{aligned} \quad (16)$$

6 *H. Tu et al.*

Similarly, the m -order derivative of $u(x)$ can also be expanded as:

$$u^{(m)}(x) = \sum_{k=0}^{\infty} \hat{u}_k^{(m)} T_k(x) \approx \sum_{k=0}^N \hat{u}_k^{(m)} T_k(x). \quad (17)$$

Consider the first derivative, due to the relationship between the Chebyshev polynomial and its derivative, there is the following relationship between \hat{u}'_k and \hat{u}_k :

$$\hat{u}'_k \approx \frac{2}{c_k} \sum_{\substack{p=k+1, \\ p+k=\text{odd}}}^N p \hat{u}_p, \quad c_k = \begin{cases} 2, & k=0 \\ 1, & \text{otherwise} \end{cases}. \quad (18)$$

In Eq. (18), the expansion coefficients can be written as a column vector, the algebraic relationship between \hat{u}'_k and \hat{u}_k can be written as a matrix, let the relationship matrix is \mathbf{D} . Then, Eq. (18) can be expressed as:

$$\hat{\mathbf{u}}' \approx \mathbf{D} \hat{\mathbf{u}}, \quad \hat{\mathbf{u}}^{(m)} \approx \mathbf{D}^m \hat{\mathbf{u}}, \quad (19)$$

where m is an arbitrary natural number, \mathbf{D} is a square matrix.

The product of two functions $u(x)$ and $v(x)$ is called a convolution term $w(x)$ in the SM. The spectral coefficients of the product of two functions have a relationship with the respective spectral coefficients:

$$\hat{w}_k \approx \frac{1}{2} \sum_{m+n=k}^N \hat{u}_m \hat{v}_n + \frac{1}{2} \sum_{|m-n|=k}^N \hat{u}_m \hat{v}_n. \quad (20)$$

The algebraic relationship between \hat{w}_k and \hat{u}_k can also be written as a matrix, and the relationship matrix can be called \mathbf{C}_v ; so the Eq. (20) becomes:

$$\hat{\mathbf{w}} \approx \mathbf{C}_v \hat{\mathbf{u}}. \quad (21)$$

3.2. Discrete PE model using CSM

In the following, we use CSM to numerically discretize operator X in Eq. (7) and p in Eq. (11). First, a linear transformation $x = 1 - 2z/H$ is used to transform the domain of the original problem from $z \in [0, H]$ to $x \in [-1, 1]$. Then, depth operator X becomes:

$$X = k_0^{-2} \left[\frac{4}{H^2} \rho(x) \frac{\partial}{\partial x} \left(\frac{1}{\rho(x)} \frac{\partial}{\partial x} \right) + k^2 - k_0^2 \right]. \quad (22)$$

Thus, Eq. (11) becomes:

$$p(r + \Delta r, x) = \exp(ik_0 \Delta r) \prod_{j=1}^n \frac{1 + \alpha_{j,n} X}{1 + \beta_{j,n} X} p(r, x). \quad (23)$$

When applying the CSM, it is necessary to consider the finite truncation of the N -term expansion of the infinite term; the problem of solving the ordinary differential problem

for an unknown function $p(r + \Delta r, x)$ is transformed to an algebraic problem with $N + 1$ unknowns. Among the available several equation-constructed methods, common methods include Tau, Galerkin and collocation methods. In this article, we mainly consider the Tau method. The Chebyshev-Tau spectral method aims to obtain the solution of the weak form of Eq. (23) (see Eq. (3.3.15) of Ref. 22 for further details):

$$\int_{-1}^1 \left[p(r + \Delta r, x) - \exp(ik_0\Delta r) \prod_{j=1}^n \frac{1 + \alpha_{j,n}X}{1 + \beta_{j,n}X} p(r, x) \right] \frac{T_k(x)}{\sqrt{1-x^2}} dx = 0, \quad (24)$$

where $k = 0, 1, 2, \dots, (N - 2)$.

In the CSM, the depth operators in Eq. (24) are processed using Eqs. (20) and (22), and the discrete depth operator X in matrix form is obtained:

$$\mathbf{X} = k_0^{-2} (\mathbf{C}_\rho \mathbf{D} \mathbf{C}_{1/\rho} \mathbf{D} + \mathbf{C}_{k^2} - k_0^2 \mathbf{I}), \quad (25)$$

where \mathbf{I} is the identity matrix; \mathbf{C}_ρ and $\mathbf{C}_{1/\rho}$ are the convolution matrices of $\rho(x)$ and $1/\rho(x)$, respectively. If the seawater density is uniform with height, then $\mathbf{C}_\rho \mathbf{C}_{1/\rho} = \mathbf{I}$. The forward Chebyshev transform is used to convert Eq. (11) from the original physical space to the spectral space with the N-term truncation approximation, and we finally obtain:

$$\hat{\mathbf{p}}(r + \Delta r, x) = \exp(ik_0\Delta r) \prod_{j=1}^n \frac{1 + \alpha_{j,n}\mathbf{X}}{1 + \beta_{j,n}\mathbf{X}} \hat{\mathbf{p}}(r, x), \quad (26)$$

where $\hat{\mathbf{p}}(r + \Delta r, x)$ and $\hat{\mathbf{p}}(r, x)$ are the column vectors that contain $N + 1$ Chebyshev spectral expansion coefficients of $p(r + \Delta r, x)$ and $p(r, x)$, respectively.

A previous study discussed the stability and convergence for the Chebyshev spectral approximation with the Tau method.²² In our problems, the stability and convergence can be assured. The boundary conditions are expanded with Eq. (16) and transformed into linear equations about expanded coefficients. When the sediment is not considered, the upper and lower boundaries of the PE model are actually pressure release boundaries, i.e.:

$$\tilde{P}(z = 0) = \tilde{P}(z = H) = 0. \quad (27)$$

From Eq. (2), $p(z = 0) = p(z = H) = 0$, and the coordinate transformation is $p(x) \Big|_{x=\pm 1} = 0$. The boundary conditions can be expressed as:

$$\sum_{k=0}^N \hat{p}_k(\pm 1)^k = 0. \quad (28)$$

In actual calculation, the constraints of the boundary conditions are reflected in the matrix equations of the original problem. The initial field $p(\Delta r)$ obtained from the self-starter¹⁷ is expanded to obtain its spectral coefficients in $\hat{p}(\Delta r)$, and the full-field $p(r, x)$ is obtained by step iteration; then, the backward Chebyshev transform is used to transform $p(r, x)$ into the original physical space to obtain $p(r, z)$, and Eq. (2) can be used to obtain the full-field acoustic pressure. Numerical dissipation is often introduced in numerical calculations

essentially due to the discrete error between two differential equations. In the FDM, the numerical dissipation depends on the precision order of the numerical discrete scheme and is unrelated to N . In the SM, the numerical dissipation depends on truncated order N : a larger N corresponds to smaller numerical dissipation, which is also the embodiment of the global approximation of the SM. Additionally, the acoustic field traditionally display by the transmission loss (TL) of the acoustic pressure, it is defined as $TL = -20 \log_{10}(p/p_0)$. The unit of TL is decibel (dB), where p_0 is the acoustic pressure at a distance of 1 m from the sound source.

4. Numerical simulation and validation

To verify the validity of the CSM in solving the PE model, the following tests and analysis are performed with two examples. To facilitate the description, the PE model program based on the CSM developed by us is abbreviated as CSMPE. The two examples represent two types of scenes: shallow water propagation with analytical solution and deep-water propagation without analytical solution. The comparison programs in the tests are the classic PE model program RAM and other programs such as KRAKEN (a classic program based on normal modes), SCOOTER (a finite element code to compute acoustic fields in range-independent environments; the method is based on direct computation of the spectral integral, and the pressure is approximated by piecewise-linear elements as are the material properties), and FFP (a fast field program implemented by the authors based on the idea of the wavenumber integration method and programmed by the finite difference method).

4.1. *An ideal fluid waveguide with a constant sound speed*

In this simple ocean waveguide model, the density of the seawater is uniform $\rho(z) = 1 \text{ g/cm}^3$, and the speed of sound underwater is unchanged ($c_0 = 1500 \text{ m/s}$) as shown in Fig. 1(a). In this case, the depth of sea is $H = 100 \text{ m}$, the sound source is located at a depth of $z_s = 36 \text{ m}$, and the sound source frequency is 20 Hz . Pressure release conditions are adopted at the surface and bottom of the sea. According to the wavenumber integration method, the exact analytical solution of this ideal fluid waveguide acoustic field is:

$$p(r, z) = \frac{2\pi i}{H} \sum_{m=1}^{\infty} \sin(k_{z_m} z_s) \sin(k_{z_m} z) H_0^{(1)}(k_{r_m} r). \quad (29)$$

Vertical wavenumber k_{z_m} and horizontal wavenumber k_{r_m} are given by the following formulas:

$$k_{z_m} = m\pi/H, \quad k_{r_m} = \sqrt{k^2 - k_{z_m}^2}, \quad m = 1, 2, \dots \quad (30)$$

Fig. 2 shows the TL fields of an ideal fluid waveguide calculated using the analytical solution, KRAKEN, RAM, and CSMPE programs. The number of terms of the rational approximation is taken as 8. In the horizontal direction, Δr in the four programs is taken as 1 m; in the vertical direction, the numbers of the discrete grid points of RAM is taken as

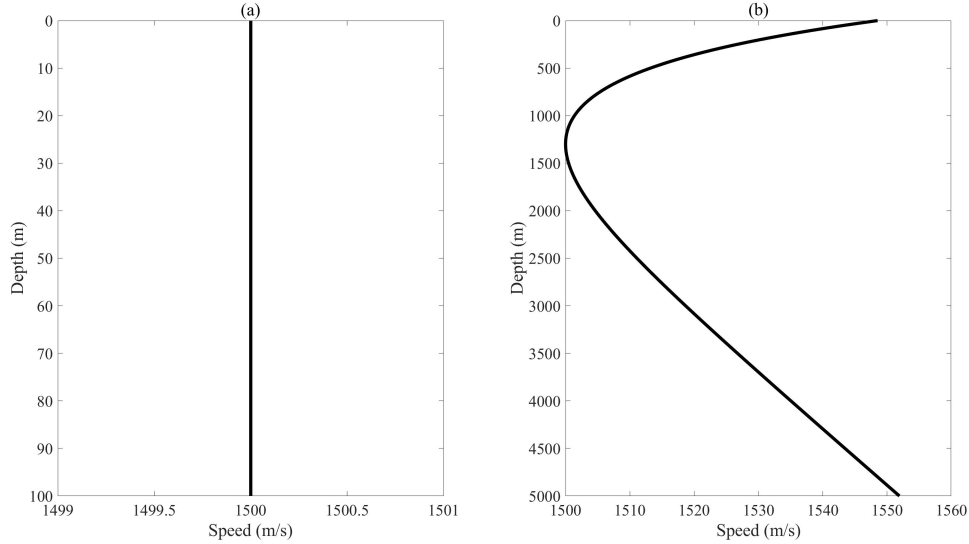


Fig. 1. Ideal fluid marine environment with constant sound speed in shallow ocean (a) and Munk sound speed profile in deep ocean (b).

200, while CSMPE takes 25 discrete points in the vertical direction, i.e., the truncated order is $N_{CSMPE}=25$. Fig. 2 shows that the TL fields calculated by the four schemes are very similar, but there are obvious differences within a horizontal distance of 500 m. Compared with the analytical solution of Fig. 2(a) and 2(c)-2(d), under near field, the results calculated by RAM and CSMPE have some distortions, which may be due to the introduction of the far-field approximation Eq. (4) in the PE model. However, the calculation results of RAM and CSMPE are very similar for the entire field, so the accuracy of the two programs must be further compared.

To compare the accuracy of the calculation results of RAM and CSMPE, Fig. 3(a) shows the TL calculated by the four programs at the depth of $z_r=36$ m. In the near-field area within 500 m from the source, the calculation results of RAM and CSMPE are significantly different from the analytical solution, but the difference between RAM and CSMPE is relatively small. In the far field, the calculation results of the TL of the four schemes are very consistent, but there are almost inconspicuous differences in the sound shadow area. Fig. 3(b) shows the zoomed portion in the shadow area in Fig. 3(a); when different numbers of discrete points are taken in the vertical direction, the errors between RAM and analytical solution are different. More precisely, the error gradually decreases when the number of grid points increases from 25 to 200. When we take 25 discrete points in the vertical direction, CSMPE is much more accurate than RAM, and there is an obvious phase error between the result of RAM and the analytical solution. When the number of discrete points gradually increases, the phase error of the RAM calculation results gradually decreases until 200 discrete points. Fig. 3(c) shows the errors between KRAKEN, RAM and CSMPE with the

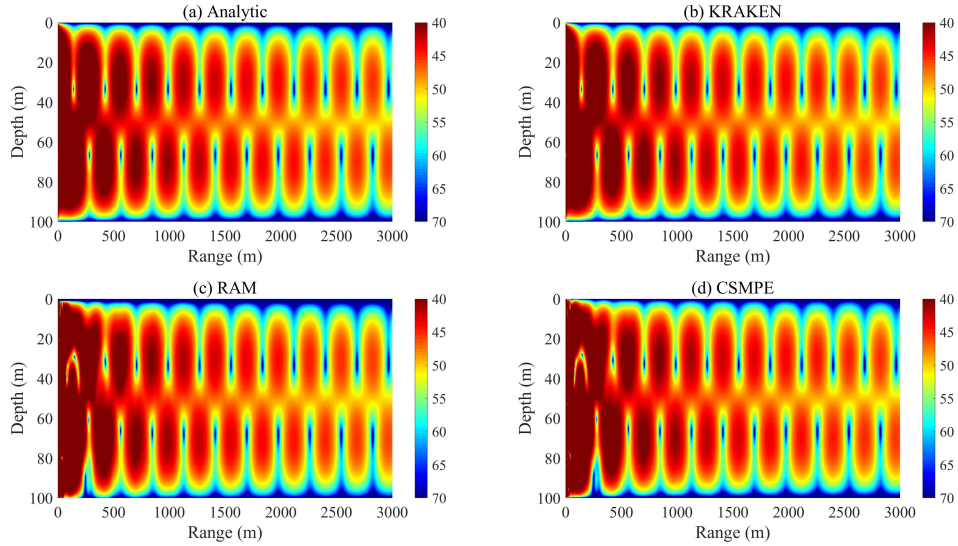


Fig. 2. TL field of an ideal fluid waveguide calculated using analytical solution (a), KRAKEN (b), RAM (c), and CSMPE (d).

analytical solution. The figure illustrates that in the near field, the calculation results of the two PE-based programs greatly differ from the analytical solution (by more than 30 dB), but the error between RAM and CSMPE is small; under identical conditions, the error of KRAKEN in the near field is very small, which further illustrates that the near-field error is generated by the PE model itself and is unrelated to the discrete method during the calculation process. In the far field, especially in the shadow area, as shown in Fig. 3(d), CSMPE has a smaller error than RAM, although RAM uses many more discrete points in the vertical direction than CSMPE (z_r is exactly on the grid point, and there is no error of TL caused by interpolation when N_{RAM} is 25, 50, 100 or 200).

Generally, in this example, compared with the analytical solution, the calculation results of both discrete methods are basically correct. Due to the far-field approximation in the PE model, the near-field calculation results have some distortion, but in the far field, the error is extremely small. Compared with the result of RAM, CSMPE has higher accuracy, and RAM uses 200 discrete points in the vertical direction, while CSMPE uses only 25 discrete points. The idea of applying the CSM to the PE model is feasible, and the calculation results are correct. CSMPE is more accurate than the classic RAM program based on FDM in these simple cases.

4.2. *An ideal fluid waveguide with a Munk sound speed profile*

This example is a deep-sea environment example. The marine hydrological environment in this case is intuitively shown in Fig. 1(b); the density of the seawater is uniform at $\rho(z) = 1$

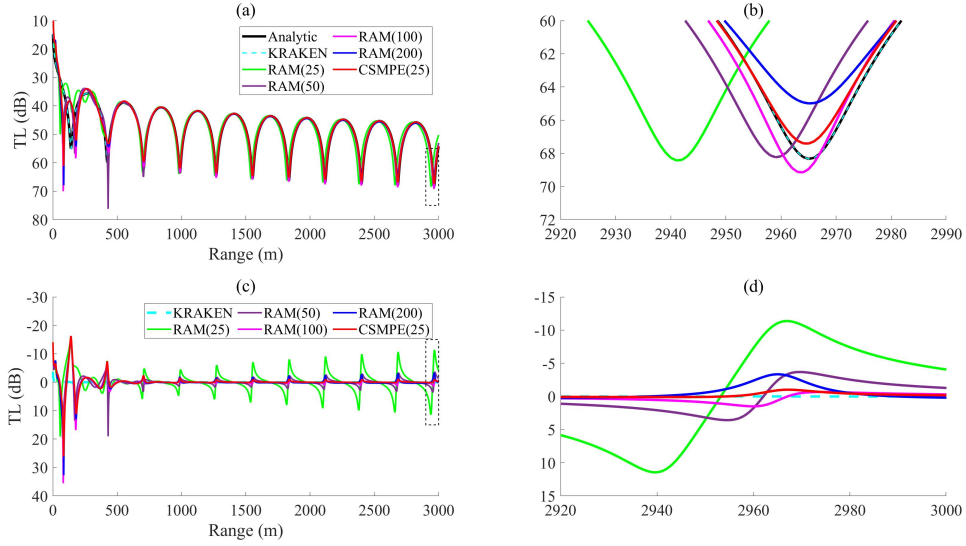


Fig. 3. TL calculated by the four programs at depth z_r (a); errors between KRAKEN, RAM and CSMPE and the analytical solution (c); (b) and (d): zoomed portions of the dotted rectangular areas in (a) and (c), respectively. The numbers 25, 50, 100 or 200 in the brackets after RAM and CSMPE in the legend correspond to the numbers of discrete points taken in the vertical direction.

g/cm^3 . The bottom of the sea is at a depth of 5000 m. We use pressure release conditions at the sea surface and bottom. The sound source is located at a depth of $z_s = 1000$ m, and the frequency of the sound source is 50 Hz. The sound speed is taken as the Munk sound speed profile, whose general form is:

$$c(z) = 1500.0 \left[1.0 + 0.0073 \left(\frac{z - 1300}{650} - 1 + \exp \left(-\frac{z - 1300}{650} \right) \right) \right]. \quad (31)$$

Since this example cannot provide an analytical solution, we can only compare the relative differences between RAM and CSMPE. We also calculate this example with SCOOTER and FFP, and we use the results of both as a reference. Fig. 4 clearly shows the spatial distribution of the TL of an ideal fluid waveguide for a Munk sound speed profile calculated using the four programs. In the horizontal direction, Δr in the four programs is taken as 20 m. In the vertical direction, the distance of the discrete grid points of SCOOTER, FFP and RAM is taken as 1 m, there are 5000 discrete points in total, while CSMPE is taken with 600 discrete points in the vertical direction, i.e., the truncation order is $N_{CSMPE} = 600$; the number of terms of the rational approximation is taken as 4. As shown in the figure, the TL fields of four programs are very similar, except for FFP in the depth direction near the sound source, where these small errors maybe caused by the model approximation.

To show the differences in results of the two methods, Fig. 5(a) shows the TL calculated by the two methods at the receiving depth $z_r = 1000$ m. As shown in Fig. 5(a), in the near-field region, the calculation results of RAM and CSMPE are almost identical. When the

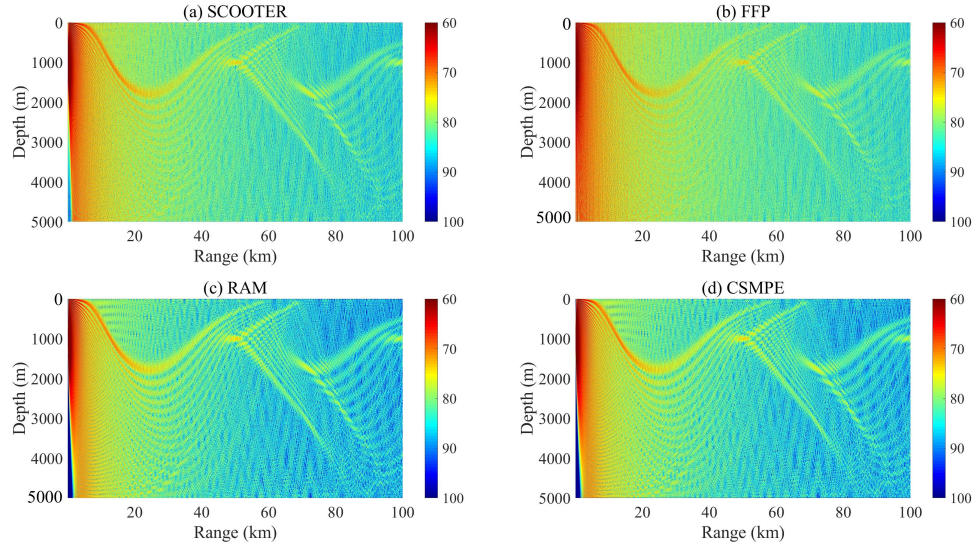
12 *H. Tu et al.*

Fig. 4. Acoustic field of an ideal fluid waveguide with a Munk sound speed profile calculated using SCOOTER (a), FFP (b), RAM (c) and CSMPE (d).

horizontal distance increases, the difference between the two programs gradually appears, and the TL curves no longer completely coincide, but the overall trends are identical. In the near field, the error between the two programs gradually increases with the distance and becomes more scattered after 20 km, and the error at a few points is larger. Figs. 5(b)-5(e) show the far-field TL at the receiving depth; although the calculation results of the two programs have a certain error, this error appears to be related to the phase. From the perspective of the entire field, the error of most points is within the acceptable range below 10 dB.

5. Analysis of the calculation time

The CSMPE program developed in this paper and RAM use the same physical framework. The difference is the different discrete methods in depth operator X . In this paper, CSM is used to discretize the depth operator of Eq. (23); therefore, we only analyze the difference in algorithmic complexity between the two programs. The process of Chebyshev forward transform and backward Chebyshev transform is added to CSMPE, and the algorithmic complexity of solving dense matrix equations is $O(N_{CSMPE}^3)$ in the “split-step”. To reduce the complexity, we conduct a preprocessing to perform an LU decomposition of the dense matrix. Although the algorithmic complexity of the LU decomposition is $O(N_{CSMPE}^3)$, it is only executed once, but the algorithmic complexity of solving the linear equations in the “split-step” is reduced to $O(N_{CSMPE}^2)$. The depth operator in RAM is discretized using Galerkin’s method based on FDM. The algorithmic complexity depends on the size (N_{RAM})

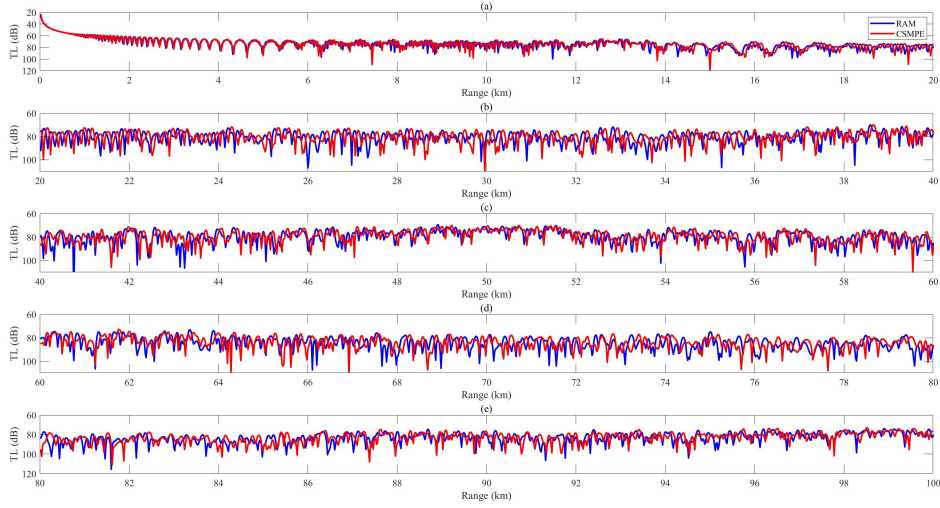


Fig. 5. TL versus range calculated by RAM and CSMPE at depth $z_r = 1000$ m.

of the tridiagonal matrix in the “split-step”. The Gaussian elimination involves sweeping downward to eliminate entries below the main diagonal followed by a back substitution sweeping upward. The algorithmic complexity of RAM is N_{RAM} . From here, CSMPE has significantly greater complexity than RAM, but the size of N_{CSMPE} in CSM is both the number of discrete points in the vertical direction and the truncated order of Chebyshev basis functions. Thus, CSM can achieve higher accuracy with fewer discrete grid points. When $N_{RAM} \gg N_{CSMPE}$, the running time of the two programs must be tested by specific examples. To compare the speed of the SM and FDM, we compare the running time of the above two examples, and the results are shown in Table 1. The listed time in the table is the average of 10 test times. In the test, MATLAB 2019a is run on a Dell XPS 8930 desktop computer equipped with an Intel i7-8700K processor, and the memory is 16 GB. Table 1

Table 1. Configuration and running time of the two examples.

Example	f	H	n	N_{RAM}	time of RAM	N_{CSMPE}	time of RAM
1	20	100	8	200	1.85 s	25	1.97 s
2	50	5000	4	5000	45.89 s	600	191.39 s

shows that in the two examples, CSM has a longer running time than RAM, while it has fewer discrete points than RAM. Thus, CSMPE is slower than RAM. Even considering that RAM is a well-optimized code, the speed of CSMPE is not satisfactory, which is the main disadvantage of CSMPE. For comparison, both examples take the density as a constant,

but in fact, CSMPE can handle the density change with depth, which can be obtained from Eq. (25).

6. Conclusion and outlook

The results of the numerical examples show that the CSMPE program can obtain higher computational accuracy with fewer discrete grid points than RAM. In fact, obtaining the expansion coefficients is equivalent to obtaining a continuous original function, while the FDM requires a larger number of discrete grid points. With approximately identical accuracy, the number of grid points in CSM is significantly smaller. This result is particularly useful for constructing a standard solution to the problem of underwater acoustic propagation in a larger spatial area. In this problem, the use of traditional FDM often requires too many spatial grids, and CSM can effectively overcome this deficiency. In the calculation of the CSMPE program, it is necessary to solve the dense matrix equations multiple times, while the FDM only must solve the large-scale tridiagonal matrix equations. Although CSMPE has much fewer vertical discrete points than RAM, it has larger calculation amount and running time than RAM.

The comparison and analysis of these simple examples show that the CSM for discrete PE model is feasible and reliable, the calculation results are credible, and CSM has higher accuracy than the classic PE model (RAM program based on the FDM) in the single layer of a body of water, but the disadvantage is the large amount of calculation.

In this paper, only the CSMPE is used to solve the simple marine environment of the flat horizontal ocean floor, and the change in sound speed profile with distance is not considered. In the future, we will attempt to generalize the CSM to solve the complicated marine environment of terrain fluctuations, special sediment and sound speed profile changes with distance based on the PE model. From another viewpoint, the CSM proposed in this paper involves solving dense matrix equations with long calculation time. In the future, it is necessary to perform in-depth performance tuning of CSMPE, use accelerators, and use parallel computing technology to accelerate its speed. For the current speed of CSMPE, it is more suitable to provide high-precision reference standards for the benchmark examples of the PE model in ocean acoustics.

Acknowledgments

This work was supported in part by the National Key Research and Development Program of China (2016YFC1401800), in part by the National Natural Science Foundation of China (61972406, 51709267), and in part by the Project of National University of Defense Technology (4345161111L).

References

1. F. B. Jensen, W. A. Kuperman, M. B. Porter and H. Schmidt, *Computational Ocean Acoustics* (Springer-Verlag, New York, 2011).

2. F. D. T. R. H. Hardin, Applications of the split-step fourier method to the numerical solution of nonlinear and variable coefficient wave equations, *SIAM Rev* **15**.
3. F. T. Tappert, *The parabolic equation approximation method in Wave Propagation and Underwater Acoustics*, volume 70 (Springer, New York, 1977).
4. R. C. C. J. A. Davis, D. White, parabolic equation workshop, Technical report, Naval Ocean Research and Development Activity, Stennis Space Center, MS, 1982.
5. R. R. Greene, The rational approximation to the acoustic wave equation with bottom interaction, *The Journal of the Acoustical Society of America* **76** (1984) 1764–1773.
6. J. F. Claerbout, *Fundamentals of Geophysical Data Processing* (Blackwell, Oxford, 1985).
7. J. S. P. D. Lee, G. Botseas, Finite-difference solution to the parabolic wave equation, *The Journal of the Acoustical Society of America* **70(3)** (1981) 795–800.
8. D. L. S. T. Mcdaniel, A finite-difference treatment of interface conditions for the parabolic wave equation: The horizontal interface, *Journal of the Acoustical Society of America* **71** (1982) 855–858.
9. K. E. G. G. Botseas, D. Lee, IFD: Wide Angle Capability, Technical report, NUSC Tech, 1983.
10. S. T. M. D. Lee, *Ocean Acoustics Propagation by Finite Difference Methods* (Pergamon, Oxford, 1988).
11. X. D. K. E. Gilbert, A fast green's function method for one-way sound propagation in the atmosphere, *Journal of the Acoustical Society of America* **94** (1993) 2343–2352.
12. E. M. Salomons, Improved green's function parabolic equation method for atmospheric sound propagation, *Journal of the Acoustical Society of America* **104** (1998) 100–111.
13. K. E. Gilbert, Eigenfunction approach to the green's function parabolic equation in outdoor sound: A tutorial, *Journal of the Acoustical Society of America* **139**.
14. L. H. A. Bamberger, B. Engquist, Higher order parabolic wave equation approximations in heterogeneous media, *SIAM J. Appl. Math.* (1988) 129–154.
15. M. D. Collins, A higher-order parabolic equation for wave propagation in an ocean overlying an elastic bottom, *Journal of the Acoustical Society of America* **86** (1989) 1459–1464.
16. M. D. Collins, Higher-order pade approximations for accurate and stable elastic parabolic equations with applications to interface wave propagation, *Journal of the Acoustical Society of America* **89** (1991) 1050–1057.
17. M. D. Collins, A self-starter for the parabolic equation method, *The Journal of the Acoustical Society of America* **92** (1992) 2069–2074.
18. M. D. Collins, A split-step pade solution for the parabolic equation method, *The Journal of the Acoustical Society of America* **93** (1993) 1736–1742.
19. M. D. Collins, The rotated parabolic equation and sloping ocean bottoms, *The Journal of the Acoustical Society of America* **87(3)** (1990) 1035–1037.
20. M. D. Collins, An energy-conserving parabolic equation for elastic media, *The Journal of the Acoustical Society of America* **94(2)** (1993) 975–982.
21. M. D. C. W. L. Siegmann, A complete energy conserving correction for the elastic parabolic equation, *Journal of the Acoustical Society of America* **105** (1999) 687–692.
22. C. Canuto, M. Y. Hussaini, A. Quarteroni and T. A. Zang, *Spectral Methods Fundamentals in Single Domains* (Spring-Verlag, Berlin, 2006).
23. R. Peyret, *Introduction to Spectral Methods* (VonKarman Institute, 1986), 1th edition.
24. X. M. Xiang, *Numerical analysis of spectral method* (Science Press, 2000), 1th edition.
25. N. P. Muravskaya, Spectral methods in physical and chemical measurements, *Journal of Physics* **1420**.
26. D. F. M. T. M. R. S. Ammi, Galerkin spectral method for the fractional nonlocal thermistor problem, *Computers and Mathematics* **73** (2017) 1077–1086.
27. N. L. Trefethen, *Finite Difference and Spectral Methods for Ordinary and Partial Differential*

16 *H. Tu et al.*

Equations (Cornell University, 1996).

28. M. J. Colbrook and L. J. Ayton, A spectral collocation method for acoustic scattering by multiple elastic plates, *Journal of Sound and Vibration* **461** (2019) 114904.
29. E. S. Wise, B. T. Cox, J. Jaros and B. E. Treeby, Representing arbitrary acoustic source and sensor distributions in fourier collocation methods, *The Journal of the Acoustical Society of America* **146** (2019) 278–288.
30. J. B. Wang and J. Pan, Acoustical wave propagator with modified Chebyshev expansion, *Computer Physics Communications* **174** (2006) 187–190.
31. R. B. Evans, A Legendre-Galerkin technique for differential eigenvalue problems with complex and discontinuous coefficients, arising in underwater acoustics, December 2016.
32. R. B. Evans, X. Di and K. E. Gilbert, A legendre-galerkin spectral method for constructing atmospheric acoustic normal modes, *The Journal of the Acoustical Society of America* **143** (2018) 3595–3601.
33. H. Tu, Y. Wang, Q. Lan, W. Liu, W. Xiao and S. Ma, A chebyshev-tau spectral method for normal modes of underwater sound propagation with a layered marine environment, *Journal of Sound and Vibration* **492** (2021) 1–16.
34. H. Tu, Y. Wang, W. Liu, X. Ma, W. Xiao and Q. Lan, A chebyshev spectral method for normal mode and parabolic equation models in underwater acoustics, *Mathematical Problems in Engineering* **2020** (2020) 1–12.